

High-resolution spectroscopy for Cepheids distance determination

II. A period-projection factor relation

N. Nardetto¹, D. Mourard², Ph. Mathias², A. Fokin^{2,3}, D. Gillet⁴

¹ Max-Planck-Institut für Radioastronomie, Auf dem Hügel 69, 53121 Bonn, Germany

² Observatoire de la Côte d’Azur, Dpt. Gemini, UMR 6203, F-06130 Grasse, France

³ Institute of Astronomy of the Russian Academy of Sciences, 48 Pjatnitskaya Str., Moscow 109017 Russia

⁴ Observatoire de Haute Provence, 04870 Saint-Michel l’Observatoire, France

Received ... ; accepted ...

ABSTRACT

Context. The projection factor is a key quantity for the interferometric Baade-Wesselink (hereafter IBW) and surface-brightness (hereafter SB) methods of determining the distance of Cepheids. Indeed, it allows a consistent combination of angular and linear diameters of the star.

Aims. We aim to determine consistent projection factors that include the dynamical structure of the Cepheids’ atmosphere.

Methods. Hydrodynamical models of δ Cep and ℓ Car have been used to validate a spectroscopic method of determining the projection factor. This method, based on the amplitude of the radial velocity curve, is applied to eight stars observed with the HARPS spectrometer. The projection factor is divided into three sub-concepts : (1) a geometrical effect, (2) the velocity gradient within the atmosphere, and (3) the relative motion of the “optical” pulsating photosphere compared to the corresponding mass elements (hereafter f_{o-g}). Both, (1) and (3) are deduced from geometrical and hydrodynamical models, respectively, while (2) is derived directly from observations.

Results. The Fe I 4896.439 Å line is found to be the best one to use in the context of IBW and SB methods. A coherent and consistent period-projection factor relation (hereafter Pp relation) is derived for this specific spectral line: $p = [-0.064 \pm 0.020] \log P + [1.376 \pm 0.023]$. This procedure is then extended to derive dynamic projection factors for any spectral line of any Cepheid.

Conclusions. This Pp relation is an important tool for removing bias in the calibration of the period-luminosity relation of Cepheids. Moreover, it reveals a new physical quantity f_{o-g} to investigate in the near future.

Key words. Techniques: spectroscopic – Stars: atmospheres – Stars: oscillations (including pulsations) – (Stars: variables): Cepheids – Stars: distances

1. Introduction

The period-luminosity relation (hereafter PL relation) of the Cepheids is the basis of the extragalactic distance scale, but its calibration is still uncertain at a $\Delta M = \pm 0.10$ mag level. Long-baseline interferometers currently provide a new, quasi-geometric way to calibrate the Cepheids PL relation. Indeed, it is now possible to determine the distance of galactic Cepheids up to 1kpc with the interferometric Baade-Wesselink method, hereafter IBW method; see for e.g. Sasselov & Karovska (1994) and Kervella et al. (2004). Interferometric measurements lead to angular diameter estimations over the whole pulsation period, while the stellar radius variations can be deduced from the integration of the pulsation velocity. The latter is linked to the observational velocity deduced from spectral line profiles by the projection factor p . In this method, angular and linear diameters have to correspond to the same physical layer in the star to correctly estimate the distance. The projection factor is currently the most important limiting quantity of the IBW method. Indeed, in addition to limb-darkening effects, it is related to the velocity gradient and, more generally, to the dynamical structure of the Cepheid atmosphere.

In 1993, Butler studied the velocity gradient in the atmosphere of four Cepheids using the excitation potential of spectral lines, together with their asymmetry. Then, Butler et al. (1996) introduced the velocity gradient in hydrostatic stellar atmosphere models and found a 20% reduction on the amplitude of the pulsation velocity curve in the case of η Aql. In addition, the γ -velocity was reduced by 2 km s⁻¹.

Fokin et al. (1996) studied the velocity gradient in the atmosphere of δ Cep, based on hydrodynamical modelling. It was found to be an important source of broadening for metallic spectral lines, being similar to rotation or geometrical projection effects.

Using an improved version of the hydrodynamical model of δ Cep, Nardetto et al. (2004, hereafter Paper I) proposed an interferometric definition of the projection factor. A difference of a few km s⁻¹ was found between the amplitude of the photospheric and line-forming region’s velocity curves, leading to a bias of 5% on the derived distance. This theoretical result has been observationally confirmed using trigonometric parallax measurements of the HST and optical long baseline interferometry by Mérand et al. (2005).

Nardetto et al. (2006a) show that spectro-interferometry provides a new geometric view of the

Cepheids’ atmosphere. However, the combination of different techniques (high-resolution spectroscopy, spectro- and differential- interferometry) is needed to efficiently constrain the physical parameters of the Cepheid atmosphere and, in particular, the projection factor.

Recently, while comparing radial velocity curves of different species, Petterson et al. (2005) found some evidence of a relation between the velocity gradient in the Cepheids’ atmosphere and their period. Using a selected sample of absorption metallic lines, we propose to probe the velocity gradient in the Cepheids’ atmosphere in order to determine *dynamic* projection factors. First, by using δ Cep and ℓ Car hydrodynamic models, we present a new spectroscopic method for determining the velocity gradient. Then, the method is applied to the eight Cepheids observed with the HARPS instrument. We discuss the choice of the spectral line and then derive a specific period-projection factor relation (hereafter *Pp* relation). Results are discussed within the framework of the *PL* relation. Finally, we propose a general method (for all lines and all stars) of determining the projection factor.

2. Cepheids observed and selected spectral lines.

Ten stars have been observed with the HARPS spectrometer ($R = 120000$): R Tra, S Cru, Y Sgr, β Dor, ζ Gem, Y Oph, RZ Vel, ℓ Car, RS Pup, and X Sgr. In the first paper of this series, Nardetto et al. (2006b, hereafter paper II) showed that the radial velocity associated with the centroid of the spectral line, together with the line asymmetry, are very important tracers of the dynamical structure of the Cepheids’ atmosphere. X Sgr was studied separately by Mathias et al. (2006) because of its very atypical behavior showing several components in the spectral lines profiles. Y Oph is not considered here due to its insufficient phase coverage (see Paper II, Fig. 3).

Using Kurucz’s models (1992), we identified about 150 unblended spectral lines. In Paper II, we considered only the unblended metallic line Fe I 6056.005 Å. In this second paper, we have carefully selected 17 spectral lines following two criteria: (1) in order to avoid bias in the determination of the line depth, the continuum must be perfectly defined for all pulsation phases and for all stars. An example of the quality required is given in paper II for the Fe I 6056.005 Å spectral line (see Fig. 1); (2) the selected sample of lines has to cover a wide range of depth. The selected spectral lines are presented in Table 1. Depending on the star and the spectral line considered, the line depth can range from 2% to 55%.

3. Hydrodynamical models.

The hydrodynamical model of δ Cep is presented in Paper I. In addition, we have derived a new, consistent model of ℓ Car. Since the main stellar quantities of ℓ Car (HD 84810) are still uncertain, we tried several sets of luminosity L , effective temperature T_{eff} , and mass M in order to get suitable observational quantities, such as the pulsation period P , the average radius of the star \bar{R} , bolometric and radial velocity curves, and the line profiles. The *ML* relation was taken from Chiosi et al. (1993), and the OPAL opacity tables (Rogers & Iglesias (1992)) were used.

This leads to the following set of parameters for a 154-zone model: $M = 11.5 M_{\odot}$, $L = 21000 L_{\odot}$, $T_{\text{eff}} = 5225 K$,

Table 1. Spectral lines used in this study.

Name	Wavelength (Å)
Fe I	4683.560
Fe I	4896.439
Fe I	5054.643
Ni I	5082.339
Fe I	5367.467
Fe I	5373.709
Fe I	5383.369
Ti II	5418.751
Fe I	5576.089
Fe I	5862.353
Fe I	6024.058
Fe I	6027.051
Fe I	6056.005
Si I	6155.134
Fe I	6252.555
Fe I	6265.134
Fe I	6336.824

Table 2. Hydrodynamical models of Cepheids.

Name	P [days]	T_{eff} [K]	$\frac{L}{L_{\odot}}$	$\frac{M}{M_{\odot}}$	$\frac{\bar{R}}{R_{\odot}}$
S Cru	4.7	5900	1900	5.6	42
δ Cep	5.4	5877	1995	4.8	43
Y Sgr	5.7	5850	2200	5.0	45
β Dor	9.9	5500	3500	5.5	65
ζ Gem	10.4	5500	3600	5.0	64
RZ Vel	21.6	5400	7450	7.0	109
ℓ Car	34.4	5225	21000	11.5	180
RS Pup	42.9	5100	22700	9.7	186

$Y = 0.28$, and $Z = 0.02$, which corresponds to a typical Pop. I chemical composition. The inner boundary has been fixed at about $T = 3.5 \cdot 10^6$ K, corresponding to 4% of the photospheric radius, so the model envelope with the atmosphere contains about 53% of the stellar mass. The atmosphere itself contains about 10^{-4} of the total stellar mass.

We started the hydrodynamical calculations with a linear, non-adiabatic fundamental-mode velocity profile having a value of 10 km s^{-1} at the surface. At the limit cycle, the pulsation period is 34.4 days, very close (3%) to the observational ($P = 35.6$ days) value deduced by Szabados et al. (1989). Bolometric and radial velocity amplitudes are 1.3 mag and 50 km s^{-1} , respectively. The relative radius amplitude at the surface is $\Delta R/R = 17\%$. The mean photospheric radius is about $\bar{R} = 180 R_{\odot}$.

For the hydrodynamical models of δ Cep and ℓ Car used in this paper (see Sect. 4), a careful analysis of the dynamical structure of their atmospheres was performed based on radiative transfer computations (under local thermal equilibrium) of all spectral lines in Table 1.

We only derived the photospheric pulsation velocity for other Cepheids (see Sect. 4.4). Thus, the physical parameters are only roughly estimated since the dynamical structure of the Cepheids’ atmosphere is not considered. The period and the radius of the Cepheids are consistent with

observations at the 2% and 3% levels respectively, while the mass follows the period-mass relation of Choisi et al. (1993) within 13%. The effective temperature and luminosity were mostly constrained by the period and the radius. R TrA was not modeled because of its extremely short period. A specific and in-depth study would be necessary to model this star.

The hydrodynamical models are presented in Table 2.

4. New insights into understanding the projection factor

In this section, we propose a division of the projection factor into sub-concepts in order to allow a direct constraint from HARPS spectroscopic observations. To test this method, we consider the hydrodynamic models of δ Cep and ℓ Car.

4.1. The projection factor definition

First of all, we have to provide a definition for the projection factor that should be applied in the IBW and SB methods. This has already been done in Paper I, but it must now be refined and adapted to the method proposed here.

We define the interferometric projection factor as

$$p = \frac{\Delta V_p^o}{\Delta RV_c} \quad (1)$$

where ΔV_p^o is the amplitude of the pulsation velocity curve associated to the photosphere (subscript p) of the star. It corresponds exactly to the *optical* (subscript o) barycenter of the photosphere defined by $\tau_c = 2/3$, where τ_c is the optical depth in the continuum. ΔRV_c is the amplitude of the radial velocity curve obtained with the centroid method, i.e. the first moment of the spectral line. This definition is justified for the following reasons:

First, we consider the pulsation velocity instead of the radius, as already proposed in paper I, in order to allow a direct application to spectroscopic observations.

Second, we consider velocity amplitudes to avoid difficulties related to the γ -velocity. The γ -velocity is the averaged value of the radial velocity curve over one pulsation period. This quantity depends on the line considered. Moreover, as shown in Paper I, the projection factor is mainly constrained by velocity amplitudes, which also justifies this choice.

Third, we consider the RV_c velocity instead of the radial velocity associated to the Gaussian fit method, as in Paper I. This is required for obtaining a projection factor independent of the rotation of the star and the natural width of the spectral lines (see Fig. 8, Paper II). We insist on this definition of the radial velocity since it is absolutely required to allow important comparisons between the projection factors of Cepheids.

In the next section, we consider the Fe I 4896.439 Å spectral line as a reference. But the results, in terms of consistency, can be generalized to any other spectral line. We find $p = 1.33$ for δ Cep and $p = 1.27$ for ℓ Car. These values are our references in the following. If we apply a minimization process between $V_p^o(\phi)$ and $pRV_c(\phi)$, with p the only free parameter, we find differences of 0.01, which provides a good estimate of the uncertainty on the projection factor.

4.2. Decomposition of the projection factor

We now divide the projection factor:

$$p = p_o f_{\text{grad}} f_{o-g} \quad (2)$$

into different quantities where,

- $f_{o-g} = \frac{\Delta V_p^o}{\Delta V_p^g}$, where ΔV_p^g is the gas (subscript g) velocity associated to the *optical* barycenter ($\tau_c = 2/3$) of the photosphere. Thus, f_{o-g} is linked to the distinction between the *optical* and *gas* photospheric layers. The *optical* layer is the location where the continuum and line photons are generated (e.g. the location of the photosphere). The *gas* layer is the location of some mass element in the hydrodynamic model mesh where, at some moment in time, the photosphere is located. Given that the location of the photosphere moves through different mass elements as the star pulsates, the two “layers” have different velocities, hence the necessity of the f_{o-g} definition. Indeed, the interferometer in the continuum is only sensitive to the *optical* layer.
- $f_{\text{grad}} = \frac{\Delta V_l^g}{\Delta V_1^g}$, where ΔV_1^g is the *gas* velocity associated to the optical barycenter ($\tau_l = 2/3$) of the line-forming (subscript l) region. Thus, f_{grad} is linked to the velocity gradient in the atmosphere of the star. This quantity depends on the line considered.
- $p_o = \frac{\Delta V_1^g}{\Delta RV_c}$ is the geometrical projection factor. It corresponds to an integration of the pulsation velocity field (associated with the line-forming region) projected on the line of sight and weighted by the surface brightness of the star (including limb-darkening in the spectral line). To derive p_o , we use intensity distributions in the continuum provided by the model. As described in Nardetto et al. (2006a), there is a relation between the pulsation velocity and the limb-darkening (and thus p_o): the intensity profile corresponding to the highest velocity *at contraction* is the most limb-darkened, while the profile corresponding to the highest velocity *at expansion* is the least limb-darkened. Given that our definition of p_o is related to the amplitude of radial and pulsation velocity curves, we consider the median value (peak-to-peak) of the $p_o(\phi)$ curve to derive the p_o -factor. However, considering intensity distribution *in the continuum* is an approximation. Indeed, hydrodynamic effects can result in much limb-darkening, especially at the wavelengths corresponding to spectral lines (see e.g. Marengo et al. 2003). Nevertheless, this seems to be negligible since we obtain a good decomposition of the projection factor.

To test this decomposition, we deduced these three quantities directly from the hydrodynamical model, considering the Fe I 4896.439 Å metallic line. For δ Cep, we find $f_{o-g} = 0.963$, $f_{\text{grad}} = 0.993$, and $p_o = 1.390$; and for ℓ Car $f_{o-g} = 0.944$, $f_{\text{grad}} = 0.982$, and $p_o = 1.366$. The corresponding projection factors are $p[\delta \text{ Cep}] = 0.963 * 0.993 * 1.390 = 1.33$ and $p[\ell \text{ Car}] = 0.944 * 0.982 * 1.366 = 1.27$, which correspond to our reference values. The physical decomposition of the projection factor is thus consistent.

One can notice that the p -factors presented in this paper are independent of the pulsation phase. Indeed, they correspond to a specific definition based on velocity amplitudes

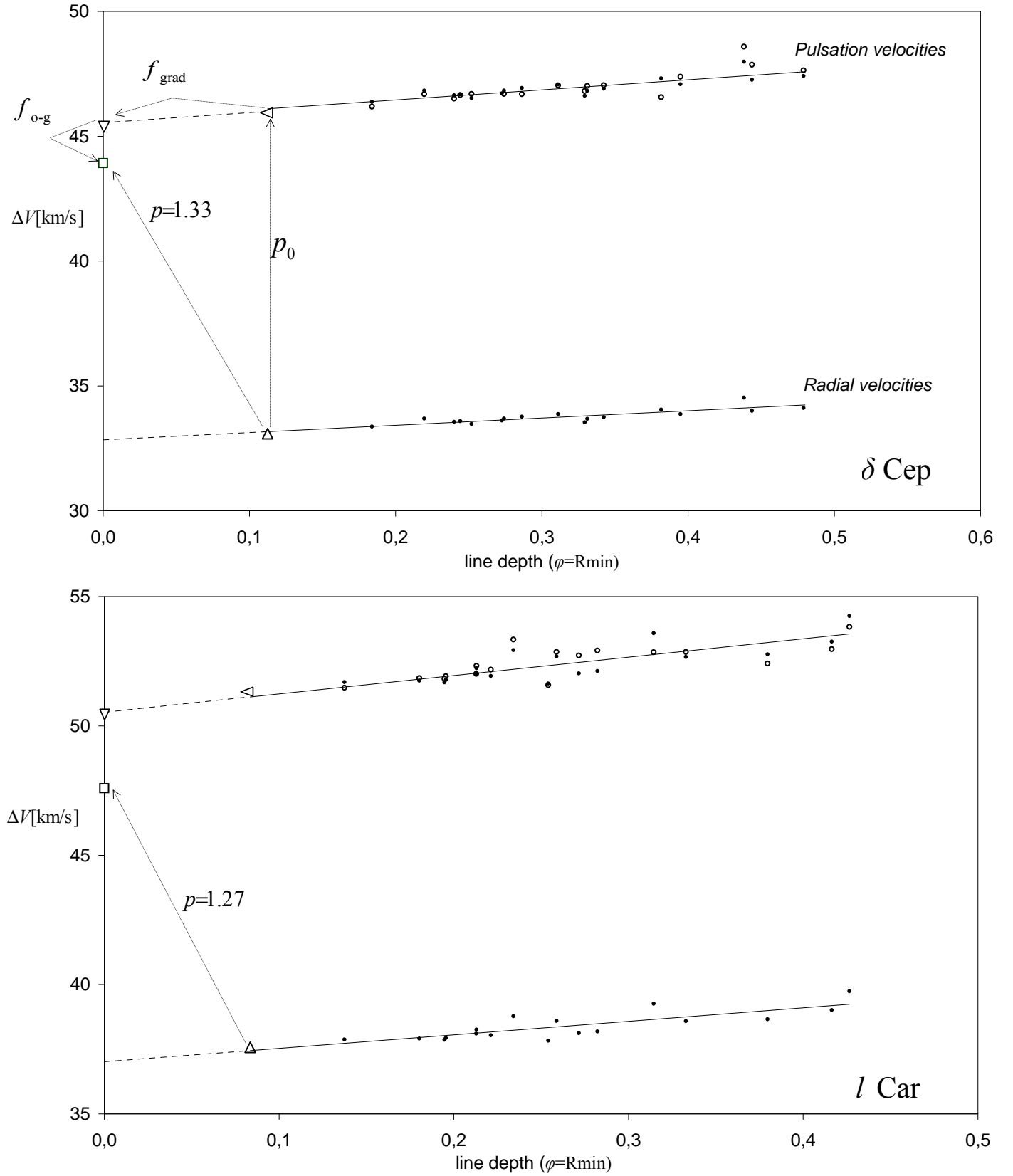


Fig. 1. The projection factor decomposition ($p = p_0 f_{\text{grad}} f_{o-g}$) in the case of the Fe I 4896.439 Å spectral line: ΔRV_c (Δ), ΔV_1^g (\triangleleft), ΔV_p^g (∇) and ΔV_p^o (\square). Reference values $p = 1.33$ and $p = 1.27$ are indicated for δ Cep and ℓ Car, respectively. The proposed method of the f_{grad} determination is to first derive ΔRV_c as a function of the line depth for all spectral lines (lower part, black points). Then, when translating (D , ΔRV_c) points into (D , $p_0 \Delta RV_c$), a new linear relation is found (upper part of the figure, black points). This new relation is (1) coherent with the pulsation velocity gradient in the atmosphere (open circles) and (2) its zero-point is consistent with the pulsation velocity corresponding to the *gaseous* layer of the photosphere: ΔV_p^g (∇).

(Eq. 1). Figure 1 represents the projection factor decomposition in the case of the Fe I 4896.439 Å line for δ Cep and ℓ Car: ΔRV_c (Δ), ΔV_1^g (\triangleleft), ΔV_p^g (∇), and ΔV_p^o (\square).

4.3. Is there a consistent way to derive f_{grad} directly from observations?

Let assume a linear relation between the line depth and the position of the line-forming region in the atmosphere of the star. Then, considering different spectral lines spread all over the atmosphere, it should be possible to determine the velocity gradient within the atmosphere. Moreover, by extrapolation to the zero line depth, it should be possible to reach the photospheric pulsation velocity.

To test these ideas, we consider the spectral line depth corresponding to the minimum extension of the star (D in the following). We discuss this choice below. Then, we derive ΔRV_c for all spectral lines in Table 1. From this quantity, one should be able to probe the velocity gradient in the atmosphere and *directly* derive f_{grad} . For that, we plot ΔRV_c as a function of the line depth for all spectral lines (Fig. 1). We find a linear correlation ($\Delta RV_c = a_0 D + b_0$) given by the following relations: $\Delta RV_c[\delta \text{ Cep}] = 2.90D + 32.84$ and $\Delta RV_c[\ell \text{ Car}] = 5.20D + 37.02$. Interestingly, these relations are spectroscopic observables.

Then, following our decomposition, we translate (D , ΔRV_c) points into (D , $p_o \Delta RV_c$) with $p_o[\delta \text{ Cep}] = 1.390$ and $p_o[\ell \text{ Car}] = 1.366$ (Fig. 1). The new relations are then: $p_o \Delta RV_c[\delta \text{ Cep}] = 4.03D + 45.64$ and $p_o \Delta RV_c[\ell \text{ Car}] = 7.10D + 50.53$. Another possible way to derive p_o , instead of using hydrodynamical modeling, is to consider a linear law for the continuum-intensity distribution of the star defined by $I(\cos(\theta)) = 1 - u_V + u_V \cos(\theta)$, where u_V is the limb-darkening of the star in the V band (Claret et al. 2000), and u_V is related to the effective temperature T_{eff} , the surface gravity $\log g$, the star metallicity, and the turbulent velocity. Using this method to derive p_o , we find that a slight correction must be applied to allow a comparison between geometric and hydrodynamic modeling. We find $p_o[\text{hydro}] = p_o[\text{geo}] - 0.010$ for δ Cep and $p_o[\text{hydro}] = p_o[\text{geo}] - 0.025$ for ℓ Car. As already mentioned, the limb-darkening in the continuum used to derive $p_o[\text{hydro}]$ is linked to the pulsation velocity and, more generally, to the whole dynamical structure of the Cepheid atmosphere. Such a dynamical effect could explain the difference that we find between $p_o[\text{hydro}]$ and $p_o[\text{geo}]$. From this, we estimate a 0.01 uncertainty on p_o . The limb-darkening (and thus p_o) will be studied in detail by interferometry in the near future.

We then overplot the amplitude of the modeled pulsation velocity curves corresponding to the different line-forming regions ΔV_1^g . Two important points have to be mentioned here.

1. The superimposition of $p_o \Delta RV_c$ and ΔV_1^g values is very satisfactory for both stars. Thus, even if the ΔRV_c quantity includes all the dynamical structure of the line-forming region (including the limb darkening), it seems, on average, to give direct access to the *gas* velocity corresponding to $\tau_1 = 2/3$, i.e. ΔV_1^g . In particular, the limb darkening (and thus the p_o -factor) seems to be independent of the spectral line considered. For any line depth D , we still have $\Delta V_1^g = p_o \Delta RV_c$.
2. We find that the zero-points of the (D , $p_o \Delta RV_c$) relations, 45.64 [δ Cep] and 50.53 [ℓ Car], are close to the ref-

erence values derived directly from the pulsation velocities of the model, $\Delta V_p^g = 45.60[\delta \text{ Cep}]$ and $50.40[\ell \text{ Car}]$. This means that, in both cases, the extrapolation to the photosphere is verified. We thus have $\Delta V_p^g = p_o b_0$. This is the key point that shows that the method proposed here is consistent and can be applied to any Cepheid. To allow this very important condition, one has to use the spectral line depth corresponding to the minimum extension of the star ($D \equiv D(\phi = R_{\text{min}})$). If another estimator is used, for example $D \equiv D(\phi = R_{\text{max}})$, or the line depth averaged over the entire pulsation cycle $D \equiv \langle D \rangle$, then the condition $\Delta V_p^g = p_o b_0$ disappears. Indeed, by extrapolating the three $p_o \Delta RV_c$ linear relations corresponding to the three estimators ($D(\phi = R_{\text{max}})$, $\langle D \rangle$, and $D(\phi = R_{\text{min}})$, respectively) towards the zero line depth, we find different agreements compared to the reference values derived directly from the variation in the photospheric pulsation velocity of the model: -1.13% , -0.70% , and 0.09% for δ Cep and -4.53% , -3.29% , and 0.25% for ℓ Car (see Fig. 2). The best extrapolation is thus obtained for the ‘minimum’ estimator. We emphasize that this result is verified for both models (δ Cep and ℓ Car) that have very different physical properties: in period (5.4d, 35.5d), radius ($43.4 R_\odot$, $180 R_\odot$), mass ($4.8 M_\odot$, $11.5 M_\odot$), and effective temperature ($5877K$, $5225K$). The ‘minimum’ estimator of the line depth (D) is used for all Cepheids in the whole paper. Considering this estimator (link to the minimum extension of the star) does not mean that our projection factors are related to any specific pulsation phase. It only means that we have to use this estimator to get the right extrapolation of the amplitude (peak-to-peak) of the pulsation velocity toward the photosphere.

Thus, taking the linear correlation $\Delta RV_c = a_0 D + b_0$ into account, we propose the following relation to observationally derive f_{grad} :

$$f_{\text{grad}} = \frac{b_0}{a_0 D + b_0} \quad (3)$$

This quantity can be derived directly from observations. In the case of our models and using the line depth corresponding to Fe I 4896.439 Å, we find $f_{\text{grad}} = 0.990$ [δ Cep] and $f_{\text{grad}} = 0.988$ [ℓ Car]. These results are very consistent with the same quantities derived directly from our projection factor decomposition. Consequently, translating these quantities into the projection factor $p = p_o f_{\text{grad}} f_{o-g}$, we find the reference values. We have thus found a new way to determine f_{grad} directly from observations.

4.4. Hydrodynamic modeling of f_{o-g}

The third quantity f_{o-g} is difficult to determine directly from observations. It requires a precise knowledge of the dynamical structure of the Cepheid atmosphere and line-forming regions. In the cases of δ Cep and ℓ Car, the model gives $f_{o-g} = 0.963$ and 0.944 , respectively.

In order to test the $P f_{o-g}$ relation, we modeled the other Cepheids of our sample (see Table 2). We only consider the velocity curves corresponding to the *optical* and *gas* photospheric layers. Consequently, no radiative transfer is calculated, and the resulting physical parameters of these models should be considered with caution. Nevertheless, these uncertainties are not critical for deriving f_{o-g} .

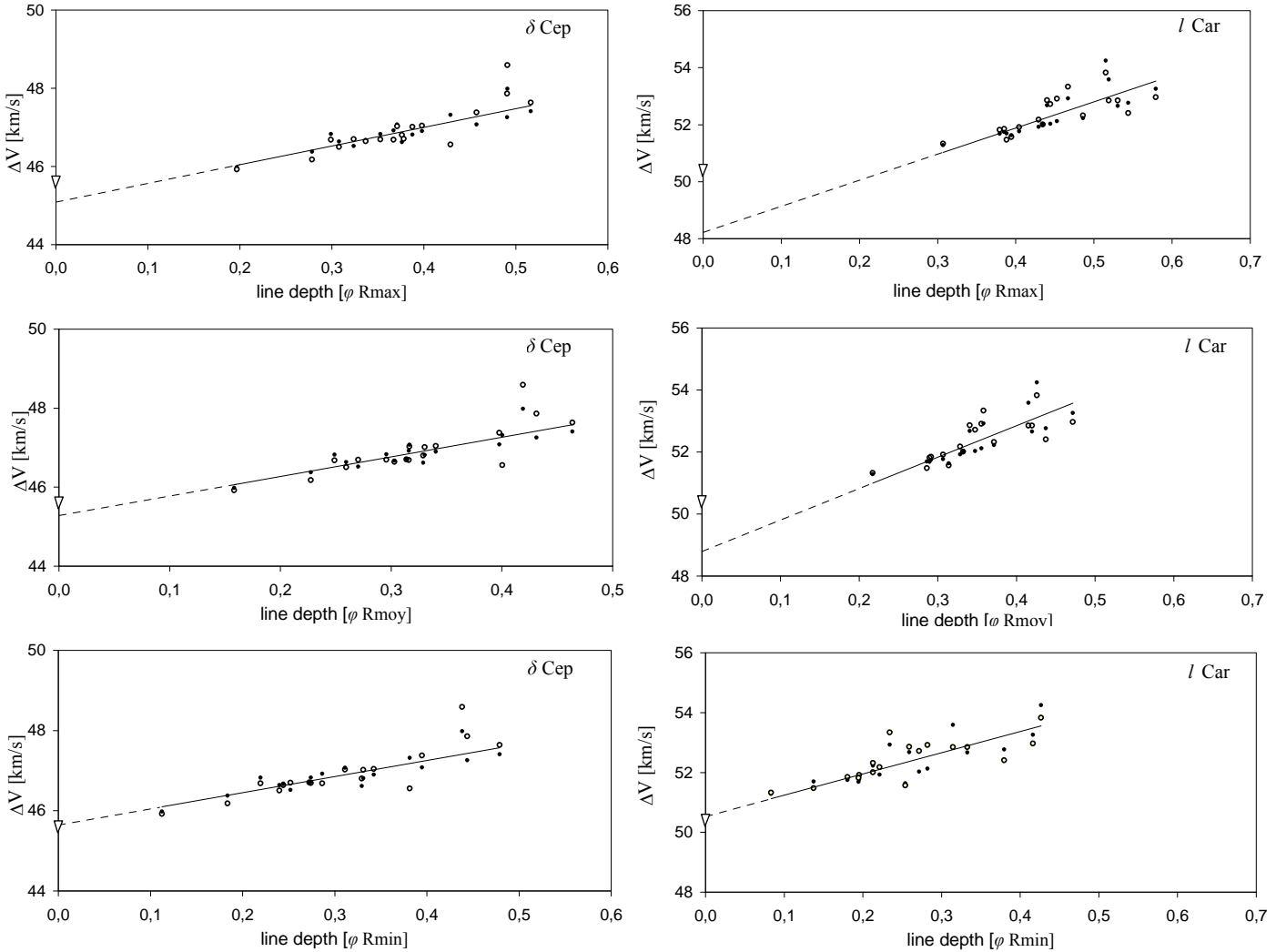


Fig. 2. ΔV_1^g (open circles) as a function of the line depth estimators $D(\phi = R_{\max})$, $\langle D \rangle$, and $D(\phi = R_{\min})$. Black points correspond to the $p_o \Delta RV_c$ quantity. The symbol ∇ indicates ΔV_p^g ; i.e., the amplitude of the photospheric pulsation velocity associated to the *gas*. We find good agreement between ΔV_1^g and $p_o \Delta RV_c$, which both present an interesting linear relation. Through extrapolation (dashed line), we find that the best estimator of the line-forming region is the line depth associated with the minimum radius, a result confirmed for δ Cep and ℓ Car hydrodynamic models.

The results are 0.966[S Cru], 0.962[Y Sgr], 0.955[β Dor], 0.953[ζ Gem], 0.951[RZ Vel], and 0.943[RS Pup]. We consider a 0.05 uncertainty on f_{o-g} .

Using these results (based on eight models), we obtain the following linear relation:

$$f_{o-g} = [-0.023 \pm 0.005] \log P + [0.979 \pm 0.005] \quad (4)$$

Using this relation we find $f_{o-g} = 0.967$ for R TrA. f_{o-g} is plotted as a function of the period in Fig. 3.

This linearity can be understood with the following picture. Let us assume two atmospheres of short- and long-period Cepheids (noted S and L) at expansion. The *gas* velocity is assumed to be the same for both atmospheres. Then, due to a geometrical effect (the radius of L is larger than the radius of S), the volume of L increases faster than S. Consequently, the density and temperature (in the adiabatic limit) also decrease faster in L. The lower atomic level of this line depopulates faster for L than for S, the opacity in the line also falls faster, the spectral line forms lower in the

atmosphere (closer to the photosphere), and finally, the *optical* radius increases less. As a consequence, the velocity of the *optical* layer decreases for a long-period Cepheid, while the *gas* velocity is supposed to be the same. This picture can be generalized at contraction and for the photospheric layer. Thus, $f_{o-g} = \frac{\Delta V_p^o}{\Delta V_p^g}$ decreases with the period of the Cepheid. Even if the $P f_{o-g}$ relation seems secured, we keep in mind that it must be studied in detail going further in our understanding of the dynamical structure of Cepheid's atmosphere. Important links between f_{o-g} , the γ -velocity, line asymmetry, and velocity gradients should be found.

5. Direct measurement of velocity gradients from HARPS observations

This section only deals with observations. For the eight stars observed, we derive RV_c and the line depth as a function of the pulsation phase for all spectral lines of Table 1. Corresponding uncertainties are estimated based on the signal-to-noise ratio.

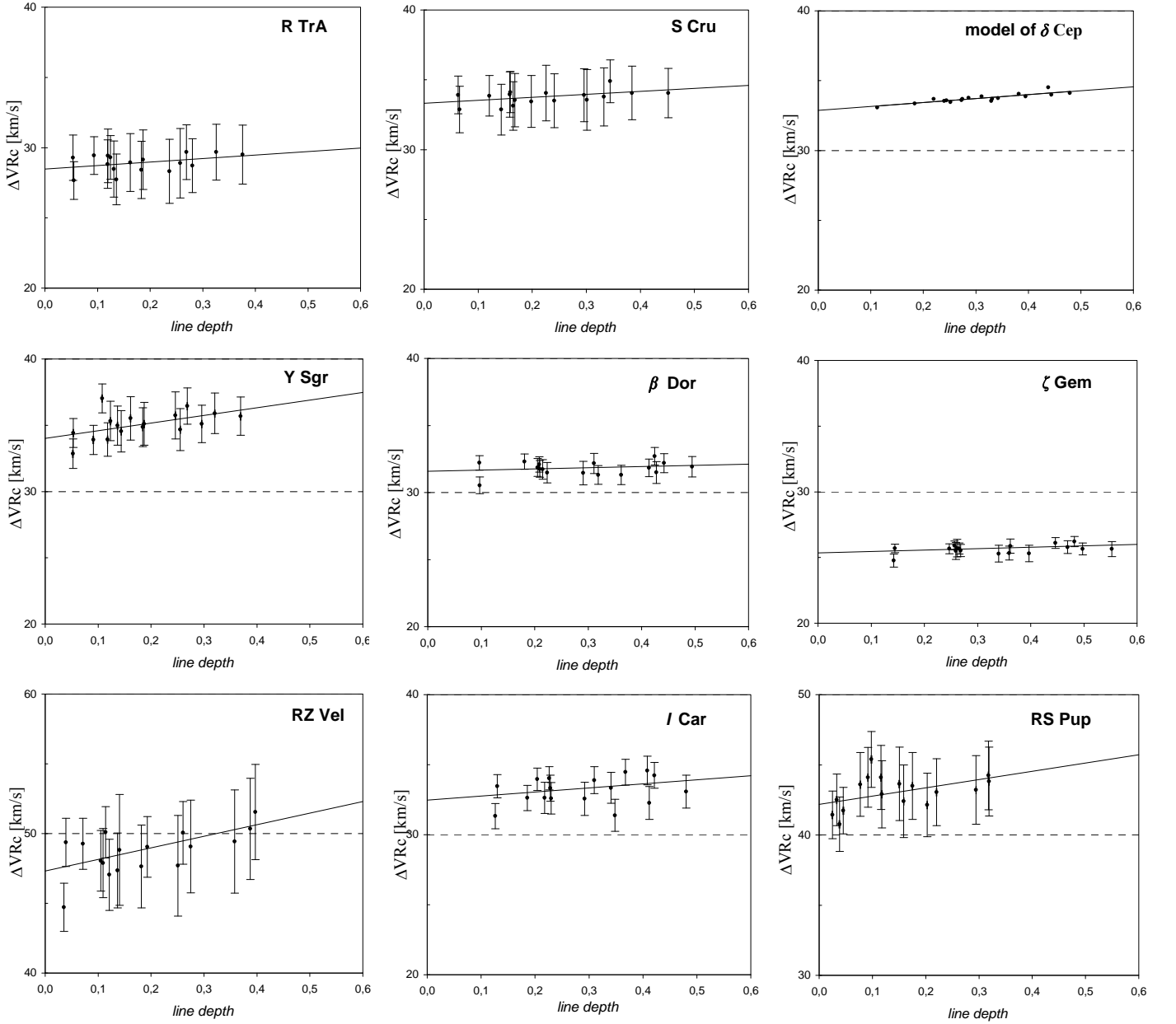


Fig. 4. ΔRV_c as a function of the depth D of the spectral line considered. Uncertainties are indicated. Stars are presented with increasing period. The δ Cep model is also indicated for comparison. Linear correlations are derived for all stars (see Tab. 3). The f_{grad} quantity is derived from these relations.

From interpolated curves (through periodic cubic spline functions), we derive $\Delta RV_c = \text{MAX}(RV_c) - \text{MIN}(RV_c)$ for all stars and lines. We also determine the pulsation phase corresponding to the minimum extension of the stars in order to derive D . ΔRV_c is represented as a function of line depth D for all stars in Fig. 4. Significant linear relations (see Table 3) are found between these two quantities. The amplitude of the velocity curves increases with the line depth (or with the position of the line-forming region in the atmosphere). This validates *a posteriori* the use of the line depth as an estimator of the line-forming region. From the coefficients provided in Table 3, we are now able to derive the f_{grad} quantity for each star using Eq. 3.

However, if one wants to compare the velocity gradient within the atmosphere of different Cepheids, the question of methodology arises. Two strategies are possible. One can

consider (1) the same line depth for all stars or (2) the same spectral line. Because a given spectral line does not have the same depth for all stars, the choice is important. We first use strategy (1) to determine which spectral lines are most fitting for the IBW method, and then consider a specific spectral line to compare the velocity gradient in the Cepheids' atmosphere.

First, we test the existence of a linear relation between $f_{\text{grad}} = \frac{b_0}{a_0 D + b_0}$ and the logarithm of the period ($\log P$) for eleven different line depths from 0 to 0.5 in increments of 0.05. By a minimization process, we obtain the relations: $f_{\text{grad}} = S(D) \log P + ZP(D)$, where the slope (S) and the zero-point (ZP) are related to the line depth considered. The variables S , ZP , and the reduced χ^2 are represented as a function of the line depth in Fig. 5. The physical interpretation of these curves is as follows.

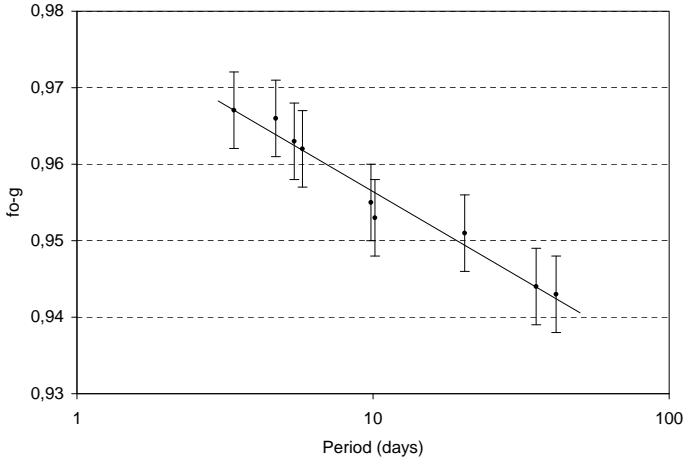


Fig. 3. f_{o-g} as a function of the period

Table 3. Linear relations between the amplitude of the velocity curves and the line depth (at minimum extension of the star), $\Delta RV_c = a_0 D + b_0$ are given for all stars, together with the 1σ uncertainty. The reduced χ^2 , defined as $\chi_{\text{red}}^2 = \frac{\chi^2}{N-\nu}$ with N the number of spectral lines and ν the number of degrees of freedom is also indicated.

Star	a_0	b_0	χ_{red}^2
R TrA	2.50 ± 4.55	28.48 ± 0.90	2
S Cru	2.13 ± 3.61	33.33 ± 0.90	2
Y Sgr	5.76 ± 3.53	34.01 ± 0.12	20
β Dor	0.86 ± 1.31	31.59 ± 0.40	9
ζ Gem	1.09 ± 0.89	25.35 ± 0.31	7
RZ Vel	8.32 ± 5.95	47.31 ± 1.02	6
l Car	2.89 ± 2.26	32.48 ± 0.67	15
RS Pup	5.89 ± 5.58	42.19 ± 0.88	4

First, for a line depth of zero, the velocity gradient is also zero for all stars (or $f_{\text{grad}} = 1$). Thus, $S = 0$, $ZP = 1$, and there is no uncertainty on f_{grad} . The reduced χ^2 is 0 since the linear relation is perfect.

Then, for low depths, the f_{grad} estimator is quite different for each star, but the effect is low and the $f_{\text{grad}} = S(D) \log P + ZP(D)$ relation is still not very sensitive to the velocity gradient. Moreover, the uncertainty on f_{grad} is low, and the same is true for S and ZP . The reduced χ^2 is good, as the linearity is well-conserved.

However, for large depths, the f_{grad} estimator becomes more and more sensitive (but also more uncertain) to the velocity gradient. The dispersion between the different stars is amplified. As a consequence, the linearity is verified at a lower level: the reduced χ^2 gets larger.

From this picture, our objective is to find the best spectral lines to use in determining f_{grad} (and then the projection factor) in the context of the IBW method. Spectral lines with depths lower than 0.1 seem to be the best choice. Such spectral lines are indeed less sensitive to the velocity gradient. It is obvious that a spectral line that forms close to the photosphere implies small differences (in velocity) between the line-forming region and the photosphere. In this case, f_{grad} is close to 1 and the corresponding uncertainty is low. Indeed, from Fig. 5, we clearly see that the uncertainties on S and ZP are decreasing for low depths.

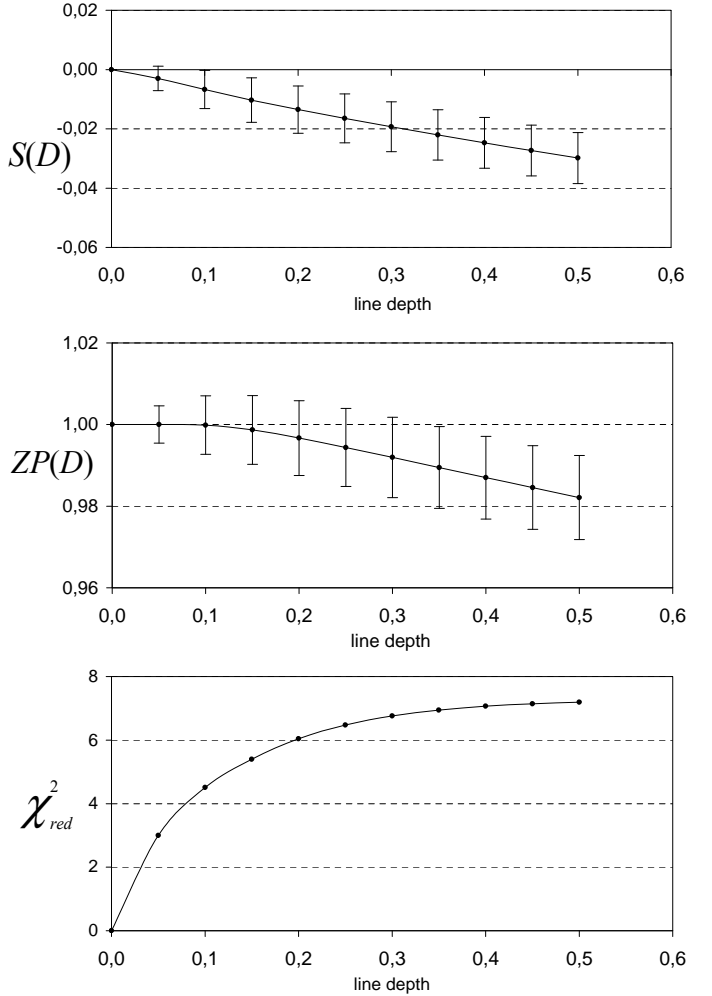


Fig. 5. Slope and zero-point of the Period- f_{grad} relation ($f_{\text{grad}} = S(D) \log P + ZP(D)$) as a function of the line depth. The reduced χ^2 is also indicated.

From Table 1, we find that the Fe I 4896.439 Å spectral line is the best. It has the lowest depth, averaged over all pulsation phases for all stars ($D = 0.08$).

In Fig. 6 we present f_{grad} as a function of the logarithm of the period for the Fe I 4896.439 Å spectral line. We obtain a linear relation between the velocity gradient and the logarithm of the period. Results are given in Table 4 for observations only (O), and for observations + the δ Cep and l Car hydrodynamical models (O+C). Consequently, we can conclude that the velocity gradient is larger in long-period Cepheids than in short-period Cepheids. Moreover, if we compare this observational result to the hydrodynamical models of δ Cep and l Car, we find very good agreement (see Fig. 6). The two models presented are thus extremely good.

6. A period-projection factor relation

We now determine the projection factors of Cepheids considering the Fe I 4896.439 Å spectral line. The p_o -factors are not determined directly using the continuum intensity distribution of the hydrodynamical models. As explained in Sect. 4.4, these models (except for δ Cep and l Car) are only used to derive f_{o-g} ; no radiative transfer in the

Table 5. Derived projections factors for all stars computed from the decomposition presented in Eq. 2.

Name	HD	P (b) [days]	p_o (c)	f_{grad} (d)	f_{o-g} (e)	p (f)
R TrA	135592	3.38925	$1.396_{\pm 0.010}$	$0.995_{\pm 0.009}$	$0.967_{\pm 0.005}$	$1.34_{\pm 0.03}$
S Cru	112044	4.68976	$1.392_{\pm 0.010}$	$0.996_{\pm 0.007}$	$0.966_{\pm 0.005}$	$1.34_{\pm 0.03}$
Y Sgr	168608	5.77338	$1.387_{\pm 0.010}$	$0.991_{\pm 0.005}$	$0.962_{\pm 0.005}$	$1.32_{\pm 0.02}$
β Dor	37350	9.84262	$1.380_{\pm 0.010}$	$0.997_{\pm 0.004}$	$0.955_{\pm 0.005}$	$1.31_{\pm 0.02}$
ζ Gem	52973	10.14960	$1.380_{\pm 0.010}$	$0.994_{\pm 0.005}$	$0.953_{\pm 0.005}$	$1.31_{\pm 0.02}$
RZ Vel	73502	20.40020	$1.375_{\pm 0.010}$	$0.994_{\pm 0.004}$	$0.951_{\pm 0.005}$	$1.30_{\pm 0.02}$
ℓ Car	84810	35.55134	$1.366_{\pm 0.010}$	$0.989_{\pm 0.005}$	$0.944_{\pm 0.005}$	$1.27_{\pm 0.02}$
RS Pup	68860	41.51500	$1.360_{\pm 0.010}$	$0.995_{\pm 0.005}$	$0.943_{\pm 0.005}$	$1.28_{\pm 0.02}$
δ Cep (a)	213306	5.419	$1.390_{\pm 0.010}$	$0.990_{\pm 0.005}$	$0.963_{\pm 0.005}$	$1.33_{\pm 0.02}$
ℓ Car (a)	84810	35.60	$1.366_{\pm 0.010}$	$0.988_{\pm 0.005}$	$0.944_{\pm 0.005}$	$1.27_{\pm 0.02}$

^a δ Cep and ℓ Car are hydrodynamical models

^b The corresponding Julian dates (T_o) can be found in Paper II.

^c p_o is derived from the linear limb-darkening laws of Claret et al. (2000) based on the static models of Kurucz (1992). We then apply a slight correction based on the δ Cep and ℓ Car hydrodynamical models: $p_o[\text{hydro}] = p_o[\text{geo}] - (0.0174 \log P - 0.0022)$ to take the dynamical structure of the Cepheid’s atmosphere into account.

^d f_{grad} is derived directly from observations using Eq 3. It is important to notice that the results indicated here correspond to the Fe I 4896.439 Å line. In the case of a modeled star, it is derived directly from the hydrodynamical model (see Sect. 4.3).

^e f_{o-g} is derived directly from the hydrodynamical models (see Sect. 4.4).

^f p -factors defined by $p = p_o f_{\text{grad}} f_{o-g}$. p_o and f_{o-g} are derived from geometrical and hydrodynamical models respectively. f_{grad} is derived from observations.

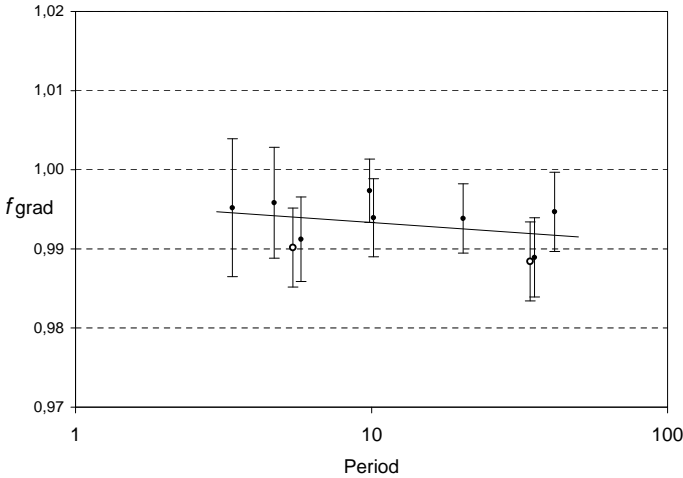


Fig. 6. f_{grad} in the case of the Fe I 4896.439 spectral line is represented as a function of the period. Open circles corresponds to the hydrodynamic models. The slope and the zero-point of the relation depend on the line depth (see Fig. 5).

Table 4. Linear relation between f_{grad} and the logarithm of the period : $f_{\text{grad}} = S \log P + ZP$ for the Fe I 4896.439 Å spectral line.

	S	ZP	χ_{red}^2
O	-0.003 ± 0.005	0.997 ± 0.006	2
O + C	-0.003 ± 0.004	0.996 ± 0.005	3

atmosphere is computed, and the observed spectral lines profiles (and radial velocity curves) are not used to constrain the models. Consequently, we are not certain about the dynamical structure of the modeled Cepheids’ atmo-

sphere and, in particular, about f_{grad} . And if f_{grad} is wrong, the limb darkening within the line (and thus the p_o -factor) could be affected. Consequently, we consider a conservative approach when deriving $p_o[\text{geo}]$ from the hydrodynamic parameters of Table 2. We then apply a slight correction: $p_o[\text{hydro}] = p_o[\text{geo}] - (0.0174 \log P - 0.0022)$ using the results based on δ Cep and ℓ Car hydrodynamic models, which were studied in detail (Sect. 3). The resulting linear relation is

$$p_o = [-0.031 \pm 0.008] \log P + [1.413 \pm 0.009]. \quad (5)$$

The f_{o-g} quantities have been deduced directly from the hydrodynamical models (see Sect. 4.4), and f_{grad} was determined from observations in the previous section. From p_o , f_{o-g} , and f_{grad} , we can now determine consistent projection factors for all stars. A summary of the results is given in Table 5 and illustrated in Fig. 7.

By combining all quantities (p_o , f_{grad} and f_{o-g}), we are able to derive a Pp relation for the first time (see Fig. 7-b). This result is a combination of observed and theoretical considerations. The resulting linear law (including observed and modeled stars) is:

$$p = [-0.064 \pm 0.020] \log P + [1.376 \pm 0.023]. \quad (6)$$

This relation holds for the Fe I 4896.439 Å spectral line, which presents the lowest line depth in our sample.

From this relation, two facts must be pointed out. First, the Pp_o relation is based on the general physical properties of Cepheids (effective temperature, surface gravity), while Pf_{grad} is derived directly from observations and states that the velocity gradient within the atmosphere is larger in long-period Cepheids. The linearity of the Pf_{o-g} relation is qualitatively understood (Sect. 4.3) and has been quantitatively verified based on eight models. Second, results concerning the δ Cep and ℓ Car hydrodynamic models are

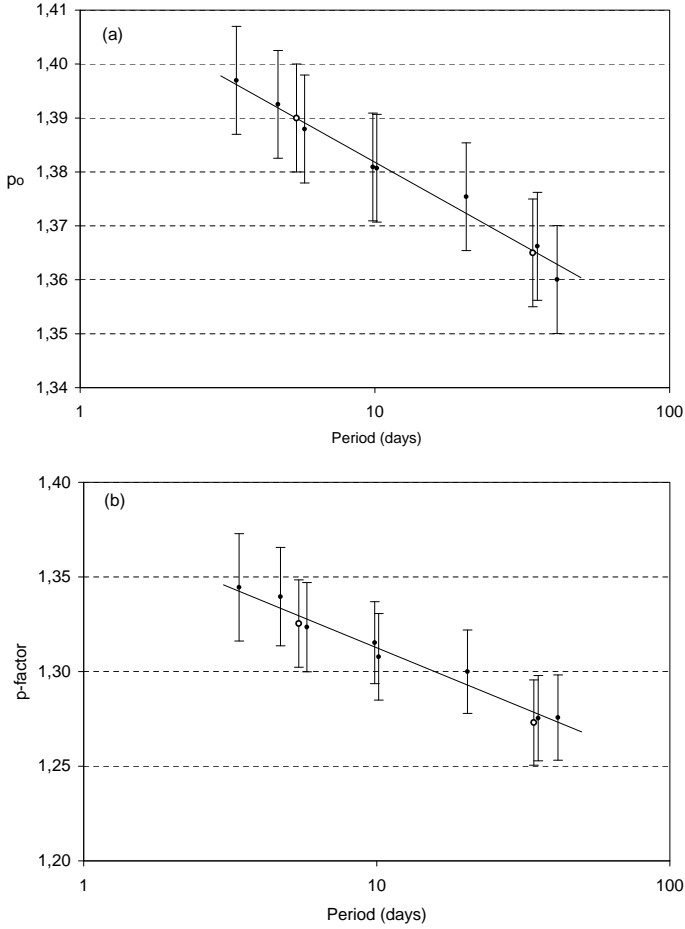


Fig. 7. The projection factor ($p = p_o f_{\text{grad}} f_{o-g}$) as a function of the logarithm of the period (diag. b), together with p_o (diag. a). Black points and open circles correspond to observations and models.

highly secured: (1) the projection factor of δ Cep was confirmed observationally by Mérand et al. (2005); (2) the velocity gradient in the atmosphere of these stars is confirmed by HARPS observations (see Sect. 5); (3) the p_o estimations are coherent at a 0.025 level with the geometrical models; and (4) from points 1, 2, and 3, we can reasonably feel secure in the estimations of f_{o-g} for δ Cep, ℓ Car, and for all stars.

7. Discussion

The derived Pp relation will be useful in the context of the IBW and SB methods. For example, if we compare Eq. 6 with the usual value widely used in the community $p = 1.36$ (Burki et al. 1982), we obtain a correction for the projection factor depending on the period. It is then possible to translate it into a bias on distances and absolute magnitudes. By this process, we obtain the relation:

$$\Delta M_V = 0.10 \log P - 0.03 \quad (7)$$

where ΔM_V is the correction to consider on the PL relation. We thus conclude that one can make an errors of 0.10 and 0.03 on the slope and zero-point of the PL relation, respectively, if $p = 1.36$ is used for all stars instead of the Pp relation. This correction is, however, only indicative

because it is indeed restricted to our definition of the projection factor (Eq. 1) and to the Fe I 4896.439 Å spectral line.

It is now possible to refine the IBW and SB methods. First, we suggest using the RV_c radial velocity to avoid bias related to the rotation velocity of the star (even if Cepheids are supposed to be slow rotators) and the width of the spectral line. One then has to determine the RV_c curve and force the average to be zero in order to avoid γ -velocity effects. Due to our careful definition of p (Eq. 1), the projection factors proposed in this paper are indeed independent of the γ -velocity. The spectral line considered must have a depth lower than 0.1 and should be the same for all considered Cepheids. The low depth of the spectral line is required to diminish the impact of the velocity gradient. If the Fe I 4896.439 Å is used, one can use Eq. 6 directly to determine the dynamic projection factors of Cepheids. If not, we propose the following method. Given the line depth of the spectral line considered for each Cepheid, it is possible to determine the f_{grad} from Table 3 and Eq. 3. If the Cepheid being studied is not in our sample, Fig. 5 can be used. Then p_o can be determined using a geometrical model. However, the consistency (at a level lower than 0.025 on p) between interferometric observations, geometrical, and hydrodynamical models should be studied in detail in the future. For f_{o-g} , one can use Eq. 4, even if this relation has to be confirmed observationally in the future. For this purpose, the development of theory and hydrodynamical models is required. Finally, the projection factor of Cepheids, following our decomposition, is $p = p_o f_{\text{grad}} f_{o-g}$. This procedure should be applied to avoid bias in the calibration of the PL relation.

However, we know that the masking cross-correlation method is widely used to increase the signal-to-noise ratio on radial velocity measurements. In that case however, one cannot exclude the impact of the rotation, the spectral lines' width, and γ -velocities effects. Nevertheless, we can still provide a Pp relation that is more appropriate considering an average line depth of $D = 0.25$. We find $p = [-0.075 \pm 0.031] \log P + [1.366 \pm 0.036]$.

Another important point is that we provide visible projection factors that should be used with visible spectroscopic observations. If one used infrared spectroscopic observations to derive the pulsation velocity, one should use specific infrared projection factors. Indeed, in the infrared, the limb darkening is supposed to be lower and the corresponding p_o -factors higher (certainly about 4%). But, spectral lines also form higher in the atmosphere (i.e. in the upper part of the atmosphere), which supposes a lower f_{grad} . More studies have to be carried out to derive an infrared Pp relation.

8. Conclusion

In the application of the IBW method, the projection factor is a key quantity. Up to now, the period-dependency of the projection factor has never been studied in detail. Here, we have presented a new spectroscopic method for directly measuring the velocity gradient in the Cepheids' atmosphere. This method has been successfully validated by the hydrodynamical models of δ Cep and ℓ Car. We find a physical relation between the period of the star and its dynamical atmospheric structure.

The models also show that the *optical* layers (observed by continuum interferometer) and the *gas* layers have to be distinguished in the interferometric definition of the projection factor. However, this quantity is still very difficult to determine directly from observations.

Combining the results obtained directly from observations and our knowledge of the dynamical structure of the δ Cep and ℓ Car atmosphere, we have been able to derive a very consistent Pp relation for the Fe I 4896.439 Å spectral line:

$$p = [-0.064 \pm 0.020] \log P + [1.376 \pm 0.023]. \quad (8)$$

We emphasize that, if a constant projection factor is used to constrain the PL relation, an error of 0.10 and 0.03 magnitudes can be done, respectively, on the slope and zero-point of the PL relation. This can even be much more if the wrong definition of the radial velocity is used or if one does not consider γ -velocity effects. We have thus presented (see discussion) a careful methodology to be applied in the context of the IBW and SB methods.

Acknowledgements. Based on observations collected at La Silla observatory, Chile, in the framework of European Southern Observatory's programs 072.D-0419 and 073.D-0136. This research made use of the SIMBAD and VIZIER databases at the CDS, Strasbourg (France). We thank C. Catala for useful discussions of the line-forming region estimator, P. Kervella for having provided the HARPS data and M. Fekety as well as Joli Adams for their careful English correction of the paper. N. Nardetto acknowledges the Max Planck Institut for Radioastronomy for financial support.

References

- Burki, G., Mayor, M., & Benz, W. 1982, *A&A*, 109, 258
 Butler, R. P. 1993, *ApJ*, 415, 323
 Butler, R. P., Bell, R. A. & Hindsley, R. B. 1996, *ApJ*, 461, 362
 Chiosi, C., Wood, P.R. & Capitanio, N. *ApJ*, 86, 541
 Claret, A. 2000, *A&A*, 363, 1081
 Fokin A.B., Gillet D. & Breitfellner M.G. 1996, *A&A*, 307, 503
 Kervella P., Nardetto N., Bersier D., et al. 2004, *A&A*, 416, 941
 Kurucz, R. L. 1992, *IAU Symp.* 149: The Stellar Populations of Galaxies, 149, 225
 Marengo, M., Karovska, M., Sasselov, D. D., et al. 2003, *ApJ*, 589, 975
 Mathias, P., Gillet, D., Fokin, A., et al. 2006, *A&A*, 457, 575M
 Mérand, A., Kervella, P., Coudé du Foresto, V. et al. 2005, *A&A*, 438, L9-L12 (Section 'Letters')
 Nardetto, N., Fokin, A., Mourard, D., et al. 2004, *A&A*, 428, 131 (Paper I)
 Nardetto, N., Fokin, A., Mourard, D., et al. 2006a, *A&A*, 454, 327
 Nardetto, N., Mourard, D., Kervella, P., et al. 2006b, *A&A* 453, 309-319 (Paper II)
 Petterson, O. K. L., Cottrell, P. L., Albrow, M. D., & Fokin, A. 2005, *MNRAS*, 362, 1167
 Rogers, F.J., & Iglesias, C.A., 1992, *ApJS*, 69, 495
 Sasselov, D. D., & Karovska, M., 1994, *ApJ*, 432, 367
 Szabados, L. 1989, *Communications of the Konkoly Observatory Hungary*, 94, 1

List of Objects

- 'R Tra' on page 2
 'S Cru' on page 2
 'Y Sgr' on page 2
 ' β Dor' on page 2
 ' ζ Gem' on page 2
 'RZ Vel' on page 2
 ' ℓ Car' on page 2
 'RS Pup' on page 2